Improving the Thermal Shock Resistance of Thermal Barrier Coatings Through Formation of an In Situ YSZ/Al$_2$O$_3$ Composite via Laser Cladding

Zohre Soleimanipour, Saeid Baghshahi, and Reza Shoja-razavi

In the present study, laser cladding of alumina on the top surface of YSZ thermal barrier coatings (TBC) was conducted via Nd:YAG pulsed laser. The thermal shock behavior of the TBC before and after laser cladding was modified by heating at 1000 °C for 15 min and quenching in cold water. Phase analysis, microstructural evaluation and elemental analysis were performed using x-ray diffractometry, scanning electron microscopy (SEM), and energy-dispersive spectroscopy. The results of thermal shock tests indicated that the failure in the conventional YSZ (not laser clad) and the laser clad coatings happened after 200 and 270 cycles, respectively. The SEM images of the samples showed that delamination and spallation occurred in both coatings as the main mechanism of failure. Formation of TGO was also observed in the fractured cross section of the samples, which is also a main reason for degradation. Thermal shock resistance in the laser clad coatings improved about 35% after cladding. The improvement is due to the presence of continuous network cracks perpendicular to the surface in the clad layer and also the thermal stability and high melting point of alumina in Al$_2$O$_3$/ZrO$_2$ composite.

1. Introduction

The durability and energy efficiency of any fuel-burning engine such as gas turbines is directly proportional to its operating temperature and oxidation resistance. In order to improve these two factors in gas turbine engines, thermal barrier coatings (TBCs) have been developed to apply on the hot sections component such as nozzle gas vanes, blades and combustors (Ref 1-5).

TBCs are advanced materials systems, mostly consisting of two layers: a metallic bond coat and a heat insulating ceramic top coat. The bond coat is an oxidation resistant metal, usually made of NiCrAlY or NiCoCrAlY alloys, which increases the bond strength between the substrate and the ceramic top coat. The most widely used ceramic top coat in TBCs is yttria-stabilized zirconia (YSZ) which exhibits excellent performance in applications such as gas turbines, and satisfies basic requirements, such as low thermal conductivity, excellent phase stability at high temperature and high thermal expansion coefficient (Ref 6-8).

The metallic bond coat is responsible for generating a third coating layer, named as thermally grown oxide (TGO), which occurs when the coating is subjected to high temperatures. The formation of TGO is due to the oxidation of the bond coat at elevated temperatures, and it is mainly made of Al$_2$O$_3$ (Ref 9, 10).

A variety of methods have been utilized to deposit TBCs on the superalloy substrates such as air plasma spraying (APS), electron-beam physical vapor deposition (EB-PVD), low-pressure plasma spraying, high-velocity oxy-fuel (HVOF), chemical vapor deposition and flame spraying (Ref 5, 11-13). Among all the mentioned methods, APS has found widespread attention due to high deposition efficiency and lower cost and consequently is the most extensively used method (Ref 6, 14-16).

Although all the progress made in the improvement of TBCs, their thermal shock resistance is still considered unsatisfactory (Ref 17). TBCs failure occurs through spallation at elevated temperatures and causes the metal substrate to come in contact with high temperature gases. It has been reported that the mismatch stresses of different layers, formation of TGO in the bond coat/top coat interface and structural transformation of zirconia from tetragonal to monoclinic are the main reasons for TBCs failure during heating cycles (Ref 18-21). Meanwhile, it has been shown the temperature gradient across YSZ coating also affects the lifetime of TBCs. In order to overcome the mentioned problem, various investigations have been conducted. Using nanostructured TBCs showed better thermal shock resistance compared to the conventional ones, because of their higher bonding strength, lower thermal conductivity and more prolonged thermal cycling lifetime (Ref 6). Laser glazing is also another promising method to increase the thermal shock resistance of TBCs, which provides a dense layer containing continuous segmented cracks perpendicular to the surface (Ref 7, 17). Previous studies showed that these segmented cracks increase the thermal shock resistance and are expected to be beneficial for accommodating the oxidation and mismatch stresses (Ref 22). Depositing an Al$_2$O$_3$ overlay on the top surface of YSZ also enhances the hot corrosion and thermal shock resistance of TBCs (Ref 23). However, due to the misfit

Zohre Soleimanipour and **Saeid Baghshahi**, Department of Materials Engineering, Science and Research Branch, Islamic Azad University, Tehran, Iran; and **Reza Shoja-razavi**, Department of Materials Engineering, Malek-Ashtar University of Technology, Shahinshahr, Isfahan, Iran. Contact e-mail: baghshahi@eng.ikiu.ac.ir.

of thermal expansion between alumina and YSZ, spallation failure occurs during the cycling process (Ref 4).

With the above background, a variety of techniques have been applied to improve the thermal shock resistance of TBC. However, laser cladding of alumina has not been studied yet. Therefore, in the present study, the authors tried to increase the thermal shock resistance of TBCs through the laser cladding of alumina over the YSZ coating, producing an in situ YSZ/Al_2O_3 composite. The thermal shock behavior of the laser clad TBCs was then studied and compared to that of the conventional YSZ

2. Materials and Methods

2.1 Materials and Coating Deposition Methods

Nickel-based super alloy Inconel 738 plates ($\Phi = 25.4$ mm$\times$6 mm) were used as substrates. Air plasma spraying (APS) (Sulzer Metco AG, Winterthur, Switzerland) was carried out to deposit a metallic bond coat and a ceramic top coat on the substrate surface. The bond and top coats are commercial NiCoCrAlY powder in a spherical shape (22 SN 6883, S.N.M.I.-Avignon, particle size 38-75 μm) and YSZ powder (7wt.% Y_2O_3-ZrO_2, Metco 204B-NS, particle size 11-125 μm), respectively. The morphology of the initial powders is shown in Fig. 1.

For laser cladding, a feed powder device was utilized. The alumina powder with the particle size of 40-100 μm (Fig. 1c) was injected directly on the top surface of coating by feeder, and the Nd:YAG pulsed laser simultaneously scanned the entire surface. APS and laser clad parameters are presented in Table 1.

2.2 Thermal Shock Test

The thermal shock tests for the coating samples were performed by the following steps:

1. Heating in the electrical furnace at 1000 for 15 min.
2. Quenching in the water, drying and putting it back to the furnace again.
3. Weighting the samples every 6 cycles and observing the surface changes of the coatings (the precision of weighting was 0.0001 g)
4. Stopping the test, when the spallation occurred approximately in 25% of the surface.

2.3 Characterization

The microstructure and morphology of the powders were characterized by a field emission scanning electron microscope (FESEM; S-4160, Hitachi, Japan). For identifying the elements, energy-dispersive spectroscopy (EDS; SAMX, VEGA\\ TESCAN, Czech Republic) was used. The surface roughness (Ra) of the coatings was measured by a roughness tester (Mitu-toyoSJ-201P, Japan).

The elastic modulus (E) of laser clad coating before and after thermal cycling was determined via Knoop indentation method. Knoop indentation tests were performed on the polished cross sections of specimens using a microhardness tester (Clemex, HT-2001, Canada). The load used was 1.96 N (200 gf), and the dwell time was 17 s. Based on Eq 1, elastic modulus was estimated by measuring the elastic recovery of the residual surface impression of the indentation diagonals as follows (Ref 6):

$$E = \frac{-\alpha H_k}{\frac{b'}{a'} - \frac{b}{a}} \qquad (Eq\ 1)$$

where H_k denotes the Knoop microhardness (Pa), b'/a' refers to the ratio of the short to long indention diagonals after elastic recovery, b/a is the ratio of the known Knoop indenter dimensions or geometry (1/7.11), and α is a constant having a value of 0.45.

Table 1 Laser cladding parameters

| Parameter	
Average power (W)	60
Pulse frequency (Hz)	30
Scanning speed (mm/s)	5
Argon flow rate (SLPMn)	10
Powder carried gas flow rate(l/min)	20
Powder feeding rate (g/min)	0.35
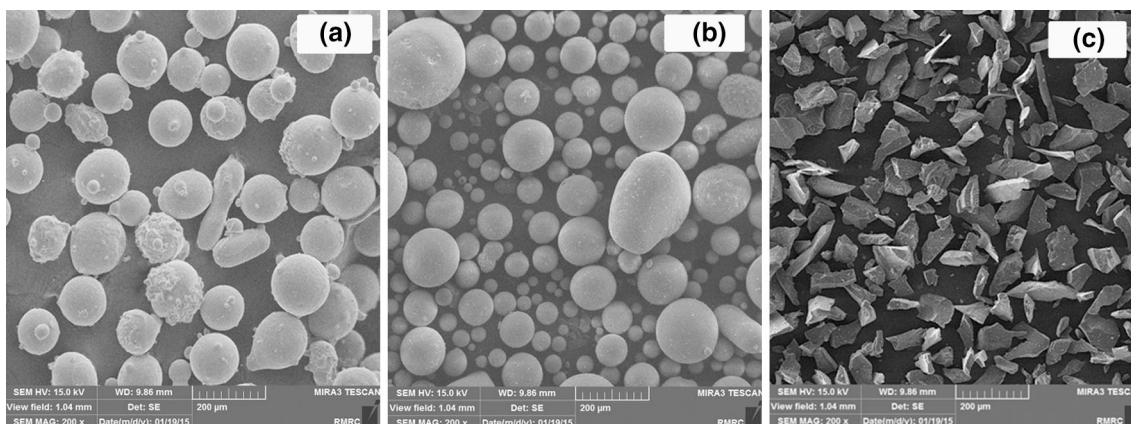
Fig. 1 FESEM micrographs NiCoCrAlY (a), conventional YSZ (b) and of Al_2O_3(c) spray powders

3. Results and Discussion

3.1 Characterization of the APS Coatings Before Thermal Cycling

The structure and composition of the interlayered APS coatings are shown in Fig. 2(a), (b), (c) and (d). The different layers of the TBC coatings are shown in Fig. 2(a). As observed, the NiCrAlY bond coat deposited on the substrate has a thickness of about 135 µm and the thickness of YSZ ceramic top coat is 360 µm. The high magnification image of the APS YSZ (Fig. 2b) revealed the columnar grains formation due to directional solidification. The microstructure of the YSZ shows some typical defects such as voids and cracks. The porosity ratio was measured to be about 11%. It can be seen from Fig. 2(c) that the top surface of YSZ is very rough and has a roughness (R_a) of about 9 µm. The roughness profile of APS coating is represented in Fig. 3.
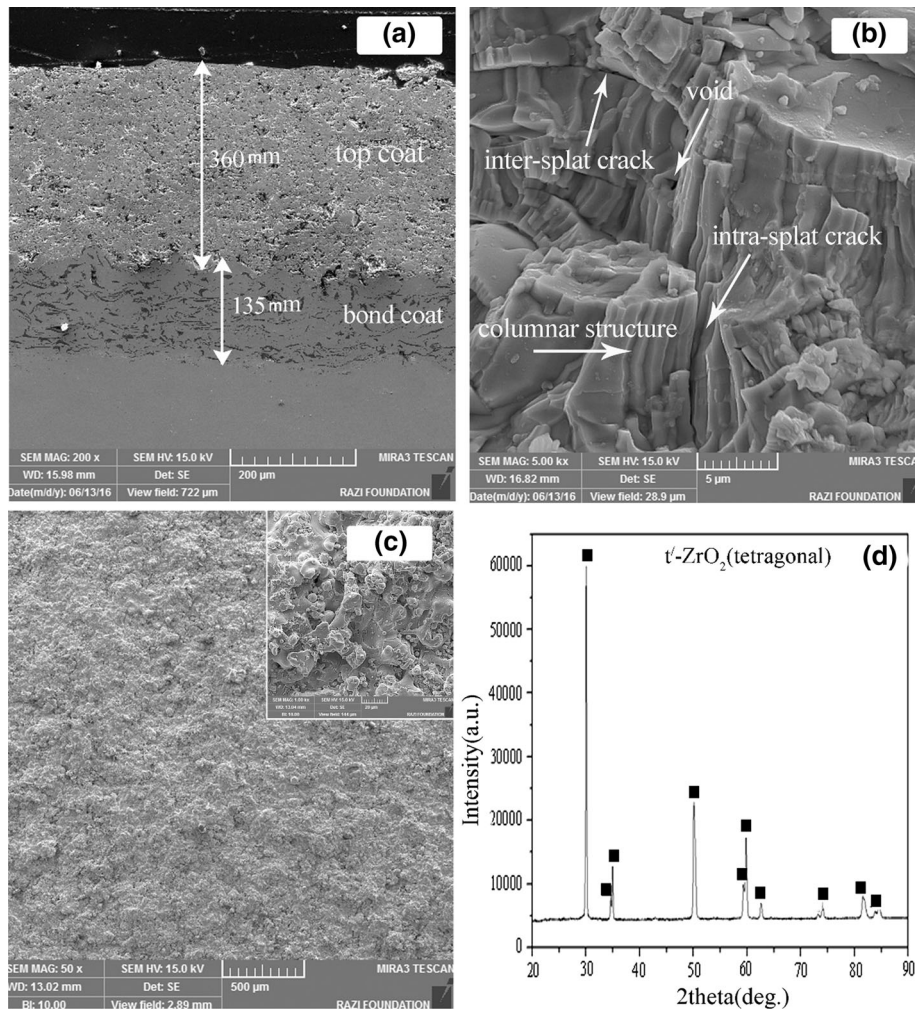
Fig. 2 FESEM micrograph of (a) the top rough surface of the sprayed coating, (b) the cross section of the sprayed coating and (c) the defects in the YSZ ceramic top coat. (d) The XRD pattern of the YSZ top coat
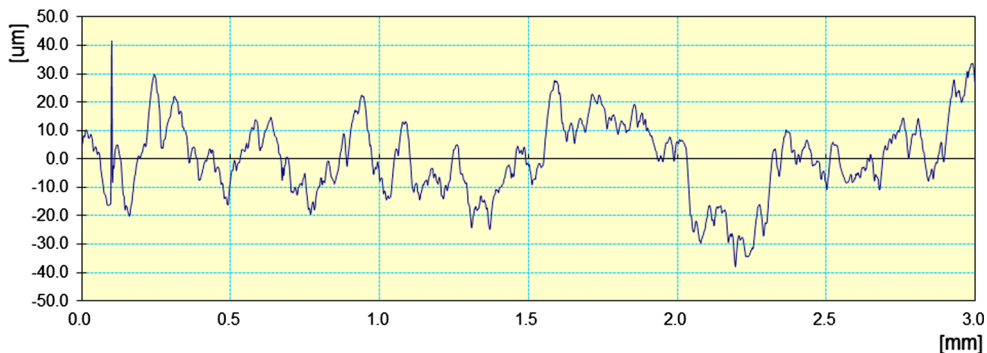
Fig. 3 Roughness profile of the conventional YSZ

The non-transformable tetragonal zirconia (t′-ZrO₂) is the only phase appearing in the YSZ coating (Fig. 2d).

3.2 Characterization of the Laser Clad Coating Before Thermal Cycling

After laser cladding of alumina on the top surface of YSZ, a dense and smooth layer with 45 μm thickness formed on the TBC coating. Figure 4 shows the schematic cross section of the laser clad coating. As shown in the figure, the clad
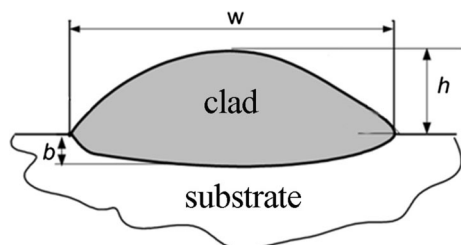

Fig. 4 Typical single-track cross-sectional morphology of the clad (Ref 25)

consists of two regions: the ceramic clad zone and the dilution zone. When dilution occurs, it means not only the alumina particles melted, but also a partial melting occurred in the YSZ layer. Calculating dilution ($d = b/b + h$) is essential to have a good understanding about the phase composition (Ref 24). In this equation, h is clad height, and b is clad depth. In the present study, the dilution ratio was calculated to be about 40%. Therefore, the molten pool comprises of both the molten alumina and the t′-ZrO₂. Since alumina is not soluble in zirconia, it forms a rigid matrix around the zirconia during the rapid solidification and prevents the phase transformation of the t′-ZrO₂ to the monoclinic structure (m- ZrO₂) during the heat cycle treatment (Ref 25).

The XRD pattern of the dense layer confirms the existence of both Al_2O_3 and ZrO_2 in the clad layer. Due to the nature of laser cladding, residual stresses were generated because of fast cooling and localized temperature gradients, which consequently led to the formation of a continuous network of segmented cracks on the clad layer and perpendicular to the surface (Figure 5a and b) (Ref 17, 26). The in situ dense Al_2O_3-YSZ composite layer has a lower roughness (7 μm) and a lower porosity ratio (4%) compared to the conventional APS YSZ. The roughness profile of laser clad coating is shown in Fig. 6.
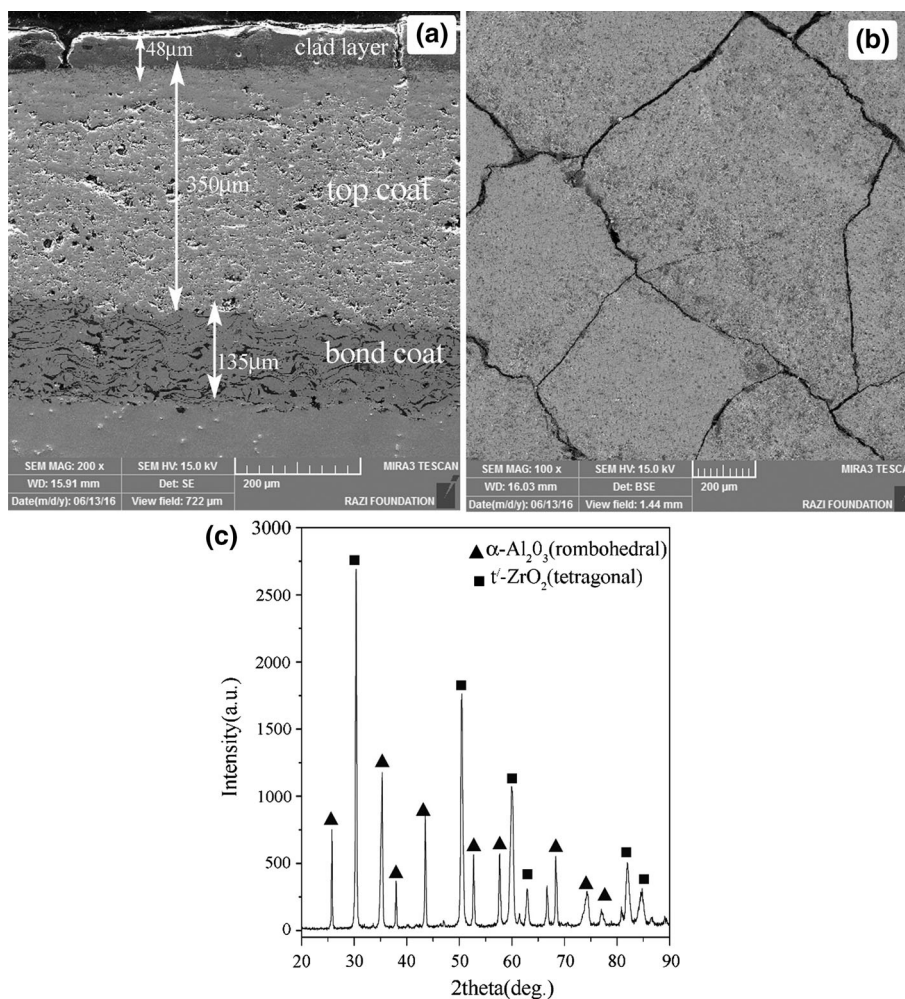

Fig. 5 FESEM image of (a) the top surface and (b) the cross section of the laser clad coating. (c) The XRD pattern of the top dense layer
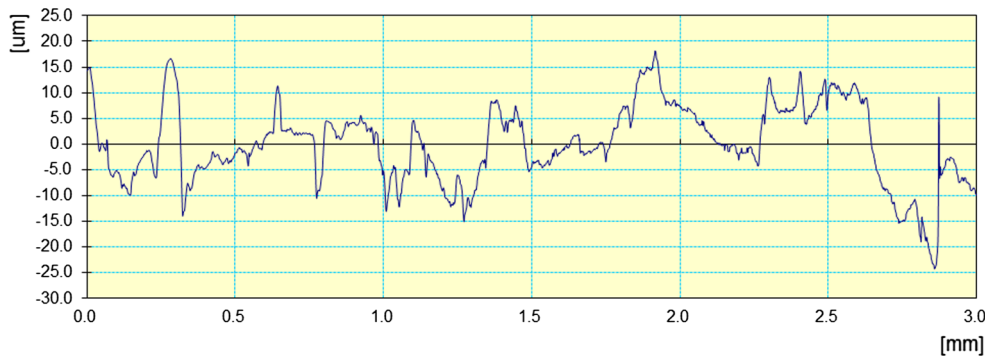
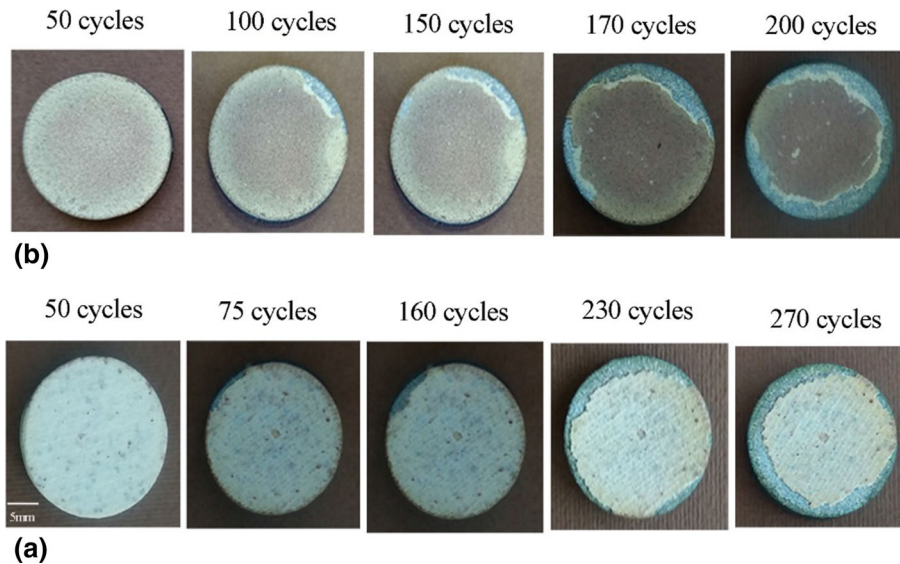**Fig. 6** Roughness profile of the laser clad sample

Fig. 7 Photographs of (a) the conventional YSZ and (b) the laser clad coating subjected to thermal shock tests
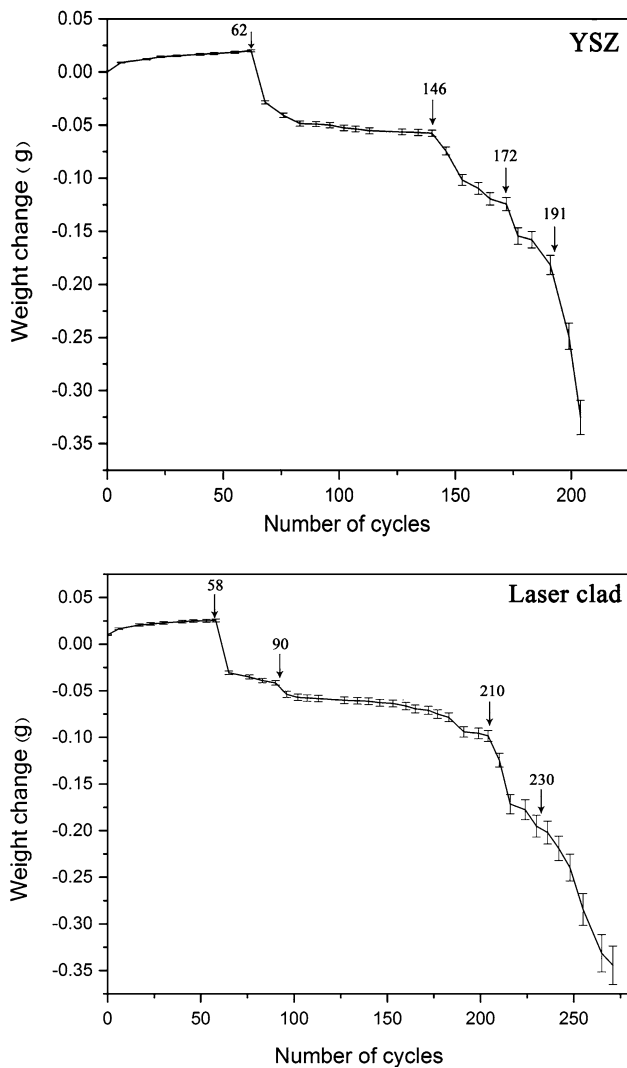
3.3 Thermal Shock Behavior of TBCs Before and After Laser Cladding

Figure 7 shows the pictures of the top surface of the conventional YSZ and the laser clad coating during thermal shock testing at different cycles. The figure reveals that in both the conventional YSZ (Fig. 7a) and laser clad coating (Fig. 7b), the failure started from the edges of the samples. Contradicted with the previous studies (Ref 6, 7), no propagation of cracks toward the inner side of the samples was observed and the failure at higher cycles continues at the outer side of the samples. Therefore, it could be alleged that "the edge effect" plays a key role in initiating the failure in the conventional YSZ and the laser clad coatings, because of the thermal stresses and fast heating and cooling condition at the edges of the samples (Ref 17). The thermal shock life of the conventional YSZ and the laser clad coatings was 200 and 270 cycles, respectively.

Figure 8 represents the weight changes versus cycle number (as a main factor of failure) for the conventional YSZ and the laser clad coating. As observed in the figure, the trend of weight loss in both coatings is the same, which means that both coatings have a similar failure mechanism. However, the laser cladding of alumina on the top surface of the YSZ has postponed the coating failure. Slight weight gain at initial cycles is due to the oxidation of the free substrate. Both diagrams show gradual and sudden weight losses. The gradual weight loss has occurred due to delamination, while the spallation is the reason for the sudden weight changes (Ref 7). Thus, two mechanisms of delamination and spallation are the main factors of TBC failure in both coatings after thermal shock tests.

3.3.1 Mechanisms of Thermal Shock Failure in the Coatings. In order to specify the failure mechanism of the YSZ coatings, the FESEM micrographs of the samples during gradual weight loss (after 100 cycle) and after the thermal shock test were investigated. Figure 9(a) belongs to the YSZ sample after 100 cycles. A horizontal crack parallel to the surface is observed in the YSZ top coat. The formation of the cracks inside the top layer confirms the delamination mechanism during the gradual weight loss of the sample in the thermal shock test. Structural defects such as voids and inter-splat cracks are the main sources for the

Fig. 8 Weight change as a function of cycle number for the plasma-sprayed and the laser clad coating

stresses arising from the thermal expansion mismatch between the ceramic top coat and the metallic bond coat. During the cyclic shock test, the thermal stresses generated the thermal expansion coefficient (TEC) mismatch of the coating layers. The thermal stress, σ_C, in the coating during cooling can be expressed by Eq 2 (Ref 27):

$$\sigma_C = \frac{-E_c(\alpha_c - \alpha_m)\Delta T}{1 - v} \qquad \text{(Eq 2)}$$
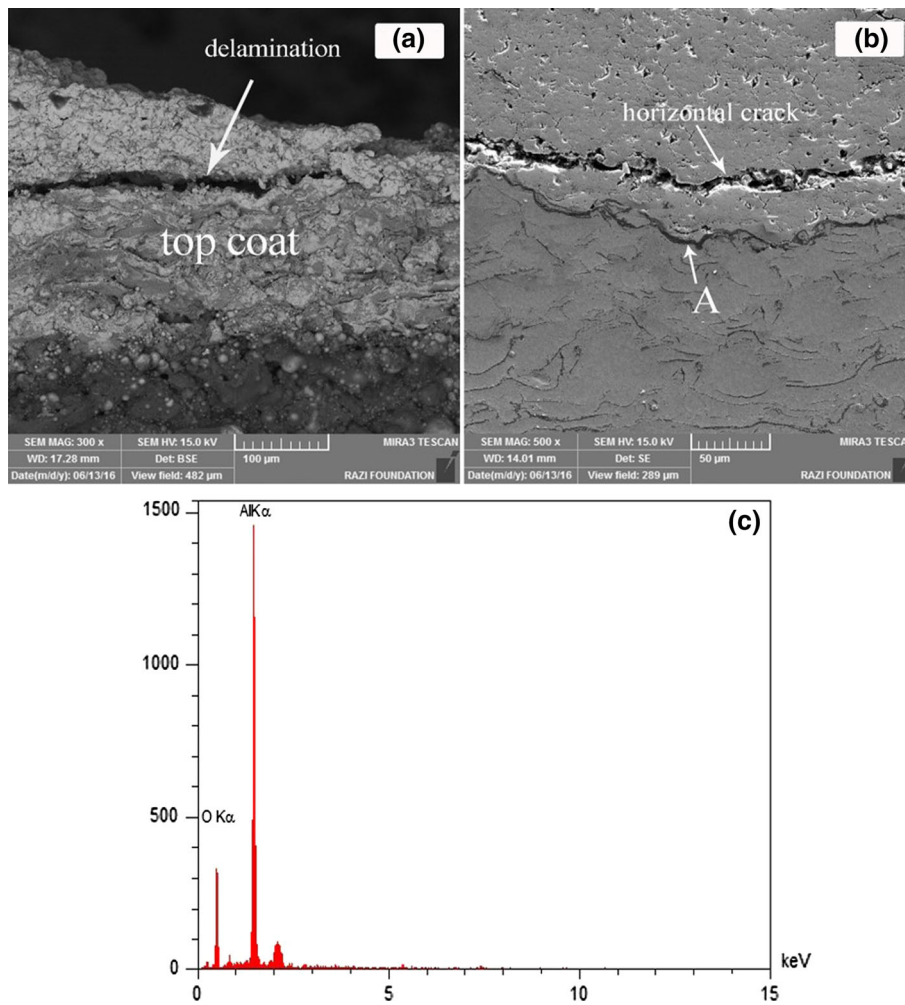
where E_c is the elastic modulus, α_c and α_m are the linear thermal expansion coefficients for the coatings, and ΔT is the change in temperature. It is reported that the average TECs for alumina, 8wt.% YSZ and NiCoCrAlY around 1000 °C are 9.6×10^{-6}, 10.7×10^{-6} and 17.5×10^{-6} °C^{-1}, respectively (Ref 28). Generally, there is little difference between thermal expansion of Al_2O_3 laser clad and YSZ layer. In contrast, the mismatch between YSZ and bond coat is high which leads to thermal stress and eventually causes the spallation. From the expression, it could be found that the stress has a linear relationship with temperature change and TEC. Therefore, in a constant temperature, the thermal stresses in YSZ/NiCoCrAlY interface are much higher than the thermal stress in YSZ-laser clad interface, leading to the formation of cracks in YSZ/NiCoCrAlY.

3.3.1.2 Effect of the Formation of TGO Layer. Figure 9(b) and 10(b) prove that a TGO layer was formed on the bond coat. The EDS analysis (Fig. 9c and 10c) showed that region A contains only Al and O, which confirms the formation of TGO as a result of oxidation of the bond coat. According to the FESEM micrograph and the EDS analysis, the TGO (the Al rich area) was formed in the both coatings.

The formation of the TGO at the interface between the top coat and the bond coat caused the localized expansion, which exerted additional tension on the YSZ surrounding the TGO, intensifying the crack growth and failure (Ref 10, 20). With increasing the intensity of the additional tension and exceeding from the amount of cohesive strength of the YSZ lamellar, there is the possibility of the propagation of cracks into the YSZ coating.

3.4 Comparison of Thermal Shock Resistance of the Plasma-Sprayed and the Laser Clad Coatings

The comparison of thermal cycling lifetimes of the plasma-sprayed and the laser clad coatings is presented in Fig. 11. As can be seen, the laser clad coating shows an excellent resistance to thermal cycling. Generally, the thermal shock resistance of the plasma-sprayed YSZ TBCs was enhanced about 35% by alumina laser cladding. Even though the failure mechanism in the conventional YSZ and the laser clad coating is the same, i.e., both caused by delamination and spallation, an improvement in thermal shock resistance is clear in the laser clad coating. Creation of a dense and impermeable layer containing continuous segmented cracks on the YSZ top coat by laser cladding decreased oxygen diffusion. Therefore, the oxidation of the bond coat and the formation of the TGO happened with a delay compared to the conventional YSZ. On the other hand, the formation of Al_2O_3-YSZ composite reduced the thermal

formation of cracks and delamination in the YSZ top coat. Figure 9(b) shows the fractured cross section of the plasma-sprayed coatings after thermal shock tests. The formation of a crack in the YSZ top coat near the top coat/bond coat interface and TGO layer in coat/bond coat interface is obvious in this figure. Figure 10(a) and (b) illustrates the fractured cross section of the laser clad coating after the thermal shock test. The formation of cracks in the clad/YSZ and the YSZ/bond coat interface and TGO layer in coat/bond coat interface is clear in this figure, which is the reason for spallation and failure. Figure 10(c) shows the EDS analysis of the region A shown in the figure.

3.3.1.1 Effect of the Coefficients of Thermal Expansion in Thermal Shock Failure. As mentioned in section 3.3.1, based on Fig. 9(b), the formation of cracks is the reason for spallation (sudden weight loss in Fig. 8), which was created by thermal

Fig. 9 FESEM micrograph of the conventional YSZ (a) after 100 cycles, (b) after failure and (c) the EDS analysis of the region A

mismatch between different layers. The existence of the segmented cracks, as mentioned earlier, accommodated thermal stresses formed due the thermal expansion mismatch between different layers (Ref 22). The high thermal stability and melting point of alumina also has a great effect on the improvement of the thermal shock resistance of the laser clad coatings.

Figure 12 presents the XRD patterns of the failed conventional YSZ and the laser clad coatings. The patterns indicate that both coatings were consisted of t'-ZrO$_2$, which means no structural transformation from tetragonal to monoclinic zirconia (m-ZrO$_2$) occurred during the thermal shock test. The t' → m transformation is accompanied by a large destructive volume change of about 6%. The stress resulting from the volume change causes delamination and spallation of the coatings. Fortunately, in this work, no phase transformation was observed during the thermal shock test.

Fracture toughness was evaluated with Eq 3 (Ref 29). The fracture toughness can be obtained by examining the surface radial cracks created during indentation, described by the equation:

$$K_{IC} = \delta \left(\frac{E}{H_v} \right)^{1/2} \frac{P}{C^{3/2}}$$

(Eq 3)

where δ is a geometric factor ($\delta = 0.016$), K_{IC} denotes the fracture toughness (MPa m$^{1/2}$), H_V is the Vickers hardness (GPa), E is the elastic modulus obtained from Eq 1 (GPa), P is the peak indentation (kgf), and $c = (c_1 + c_2)/2$ is the average length of two radial cracks (mm).

It can be seen from Eq 3 that elastic modulus and fracture toughness have direct relationship. The hardness, elastic modulus and fracture toughness of the samples are given in Table 2. As indicated in the table, the hardness, young modulus and fracture toughness decreased after thermal cycling, which is due to the formation of a defective structure with porosity and cracks (Ref 30, 31). Therefore, the reduction in modulus after thermal cycling resulted in a decrease in fracture toughness. Also, the reduction in fracture toughness could be attributed to the lack of residual stress release in the coating after thermal cycling. It has been reported that the release of residual stresses enhances the coatings fracture toughness and
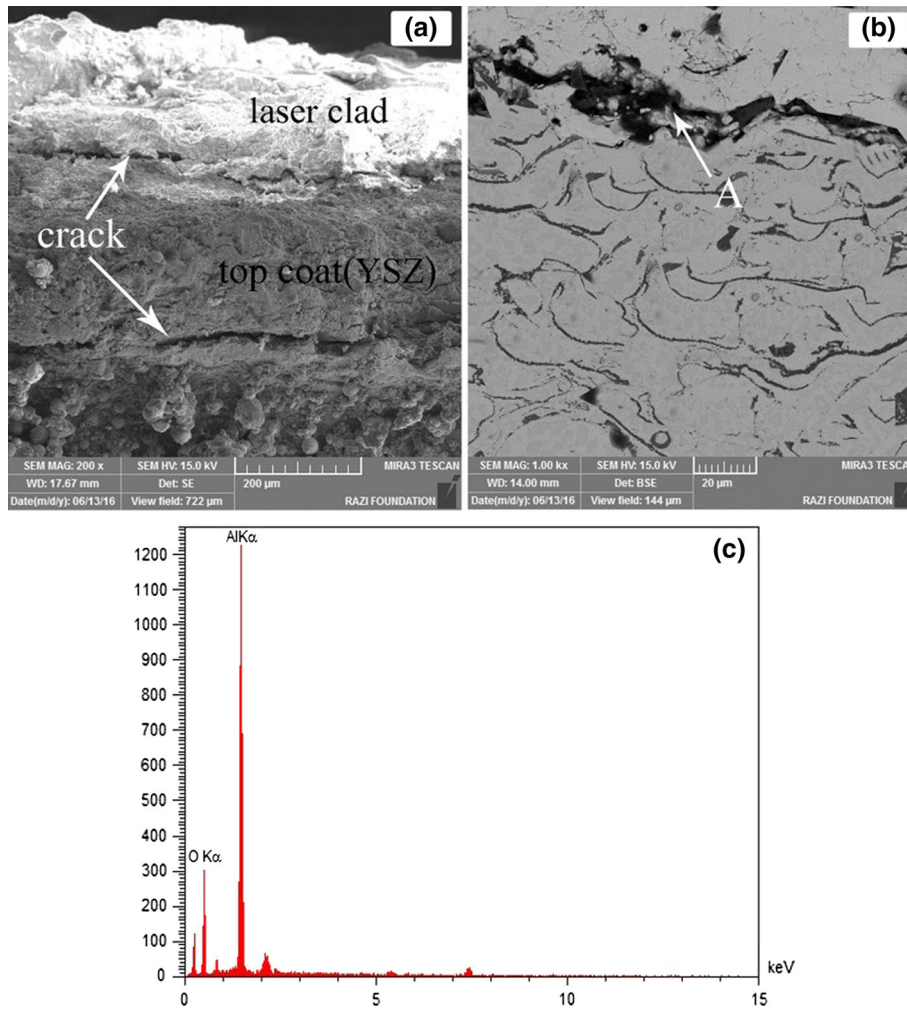
Fig. 10 (a, b) The FESEM micrographs of the fractured cross section of the laser clad coatings after thermal shock testing at two different magnifications and (c) the EDS analysis of the region A
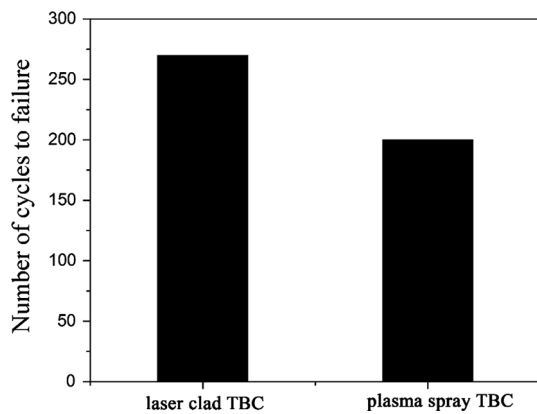
Fig. 11 Thermal cycling lifetime of the laser clad and plasma-sprayed TBCs

leads to the improvement of the coatings' performance (Ref 31, 32). Therefore, it can be said that K_{IC} and residual stress have inverse relationship.
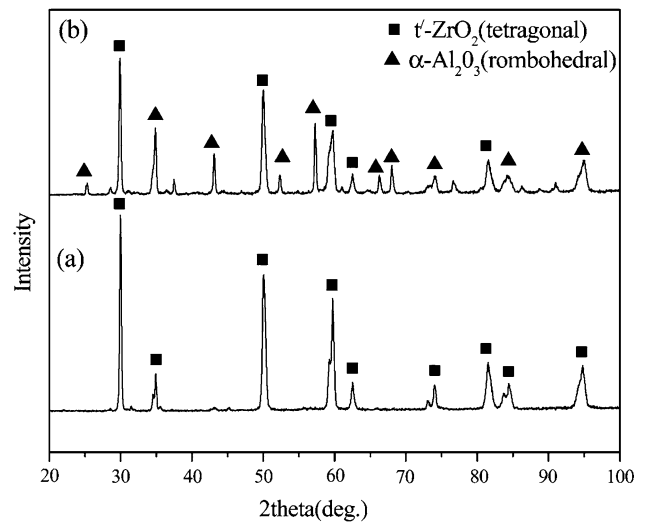
Fig. 12 XRD pattern of (a) the conventional YSZ and (b) the laser clad coating after the thermal shock test

Table 2 Hardness, young modulus and fracture toughness of laser clad coating before and after thermal shock cycles

Samples	H_k, Gpa	E, Gpa	K_{IC}, Mpa $\sqrt{m}^{-1}$
Laser clad before thermal cycling	1018	8633.40	236.65
Laser clad after thermal cycling	284.34	1146.15	220.51

4. Conclusion

Alumina laser cladding of air plasma-sprayed YSZ on the In738LC was successfully performed in the current investigation. The thermal shock behavior of the coatings before and after laser cladding was studied. The following conclusions may be drawn from the investigation:

1. A dense, smooth and impermeable layer with the thickness of about 45 μm, containing continuous segmented cracks formed on the top surface of the YSZ after laser clad coating.
2. Thermal shock resistance of the laser clad coating had a 35% increase compared with the conventional YSZ.
3. The failure mechanism of the TBCs before and after laser cladding was the same and was created by delamination and spallation.
4. The oxidation of the bond coat and the formation of the TGO was observed in the bond coat/top coat interface in both the conventional YSZ and the laser clad coatings.
5. Hardness, Young Modulus and fracture toughness of laser clad coating after thermal shock cycles significantly reduced.

References

1. N.V. Patel, E.H. Jordan, S. Sridharan, and M. Gell, Cyclic Furnace Testing and Life Predictions of Thermal Barrier Coating Spallation Subject to a Step Change in Temperature or in Cycle Duration, *Surf. Coat. Technol.*, 2015, **275**, p 384–391
2. M. Zhaia, D. Lia, Y. Zhao, X. Zhong, F. Shao, H. Zhao, C. Liu, and S. Tao, Comparative Study on Thermal Shock Behavior of Thick Thermal Barrier Coatings Fabricated with Nano-Based YSZ Suspension and Agglomerated Particles, *Ceram. Int.*, 2016, **42**, p 12172–12179
3. J. Wu, H.B. Guo, L. Zhou, L. Wang, and S.K. Gong, Microstructure and Thermal Properties of Plasma Sprayed Thermal Barrier Coatings from Nanostructured YSZ, *J. Therm. Spray Technol.*, 2010, **19**, p 1186–1194
4. R. Liu, S. Yuan, Z. Wang, Y. Zhao, M. Zhang, and L. Shi, Graded YSZ/Al₂O₃ Hot Corrosion Resistant Coating with Enhanced Thermal Shock Resistance, *RSC Adv.*, 2013, **3**, p 17034–17038
5. X. Song, Z. Liu, T. Suhonen, T. Varis, L. Huang, X. Zheng, and Y. Zeng, Effect of Melting State on the Thermal Shock Resistance and Thermal Conductivity of APS ZrO₂-7.5 wt.% Y₂O₃ Coatings, *Surf. Coat. Technol.*, 2015, **270**, p 132–138
6. H. Jamali, R. Mozafarinia, R. Shoja Razavi, and R. Ahmadi-Pidani, Comparison of Thermal Shock Resistances of Plasma-Sprayed Nanostructured and Conventional Yttria Stabilized Zirconia Thermal Barrier Coatings, *Ceram. Int.*, 2012, **38**, p 6705–6712
7. R. Ghasemin, R. Shoja-Razavi, R. Mozafarinia, and H. Jamali, The Influence of Laser Treatment on Thermal Shock Resistance of Plasma-Sprayed Nanostructured Yttria Stabilized Zirconia Thermal Barrier Coatings, *Ceram. Int.*, 2014, **40**, p 347–355
8. C. Giolli, A. Scrivani, G. Rizzi, F. Borgioli, G. Bolelli, and L. Lusvarghi, Failure Mechanism for Thermal Fatigue of Thermal Barrier Coating Systems, *J. Therm. Spray Technol.*, 2009, **18**, p 223–230
9. R. Eriksson, H. Brodin, S. Johansson, L. Östergren, and X.H. Li, Fractographic and Microstructural Study of Isothermally and Cyclically Heat Treated Thermal Barrier Coatings, *Surf. Coat. Technol.*, 2014, **243**, p 82–90
10. N.M. Yanar, G.H. Meier, and F.S. Pettit, The Influence of Platinum on the Failure of EBPVD YSZ TBCs on NiCoCrAlY Bond Coats, *Scr. Mater.*, 2002, **46**, p 325–330
11. S. Guo and Y. Kagawa, Isothermal and Cycle Properties of EB-PVD Yttria-Partially-Stabilized Zirconia Thermal Barrier Coatings at 1150 and 1300 °C, *Ceram. Int.*, 2007, **33**, p 373–378
12. T.A. Dobbins, R. Knight, and M.J. Mayo, HVOF Thermal Spray Deposited Y₂O₃-Stabilized ZrO₂ Coatings for Thermal Barrier Applications, *J. Therm. Spray Technol.*, 2003, **12**, p 214–225
13. J.R.V. Garcial and T. Goto, Thermal Barrier Coatings Produced by Chemical Vapor Deposition, *Sci. Technol. Adv. Mater.*, 2003, **4**, p 397–402
14. X. Chen, Y. Zhao, X. Fan, Y. Liu, B. Zou, Y. Wang, H. Ma, and X. Cao, Thermal Cycling Failure of New LaMgAl₁₁O₁₉/YSZ Double Ceramic Top Coat Thermal Barrier Coating Systems, *Surf. Coat. Technol.*, 2011, **205**, p 3293–3300
15. Y. Bai, Z.H. Han, H.Q. Li, C. Xu, Y.L. Xu, Z. Wang, C.H. Ding, and J.F. Yan, High Performance Nanostructured ZrO₂ Based Thermal Barrier Coatings Deposited by High Efficiency Supersonic Plasma Spraying, *Appl. Surf. Sci.*, 2011, **257**, p 7210–7216
16. E. Sanchez, E. Bannier, V. Cantavella, M.D. Salvador, E. Klyatskina, J.Grzonka Morgiel, and A.R. Boccaccini, Deposition of Al₂O₃-TiO₂ Nanostructured Powders by Atmospheric Plasma Spraying, *J. Therm. Spray Technol.*, 2008, **17**, p 329–337
17. R. Ahmadi-Pidani, R. Shoja-Razavi, R. Mozafarinia, and H. Jamali, Improving the Thermal Shock Resistance of Plasma Sprayed CYSZ Thermal Barrier Coatings by Laser Surface Modification, *Opt. Lasers Eng.*, 2012, **50**, p 780–786
18. Q. Cui, S.M. Seo, Y.S. Yoo, Z. Lu, and S.W. Myoung, Thermal Durability of Thermal Barrier Coatings with Bond Coat Composition in Cyclic Thermal Exposure, *Surf. Coat. Technol.*, 2015, **284**, p 69–74
19. H. Dong, G.J. Yang, H.N. Cai, H. Ding, C.X. Li, and C.J. Li, The Influence of Temperature Gradient Across YSZ on Thermal Cyclic Lifetime of Plasma-Sprayed Thermal Barrier Coatings, *Ceram. Int.*, 2015, **41**, p 11046–11056
20. M.R. Begley and H.N.G. Wadley, Delamination Resistance of Thermal Barrier Coatings Containing Embedded Ductile Layers, *Acta Mater.*, 2012, **60**, p 2497–2508
21. X. Zhong, H. Zhao, C. Liu, L. Wang, and F. Shao, Improvement in Thermal Shock Resistance of Gadolinium Zirconate Coating by Addition of Nanostructured Yttria Partially-Stabilized Zirconia, *Ceram. Int.*, 2015, **41**, p 7318–7324
22. J.H. Lee, P.C. Tsai, and C.L. Chang, Microstructure and Thermal Cyclic Performance of Laser Glazed Plasma-Sprayed Ceria-Yttria-Stabilized Zirconia Thermal Barrier Coatings, *Surf. Coat. Technol.*, 2008, **202**, p 5607–5612
23. C. Ren, Y.D. He, and D.R. Wang, Cyclic Oxidation Behavior and Thermal Barrier Effect of YSZ-(Al₂O₃/YAG) Double-Layer TBCs Prepared by the Composite Sol-Gel Method, *Surf. Coat. Technol.*, 2011, **206**, p 1461–1468
24. J.D. Kim and Y. Peng, Melt pool Shape and Dilution of Laser Cladding with Wire Feeding, *J. Mater. Process. Technol.*, 2000, **104**, p 284–293
25. A. Afrasiabi, M. Saremi, and A. Kobayashi, A Comparative Study on Hot Corrosion Resistance of Three Types of Thermal Barrier Coatings: YSZ, YSZ + Al₂O₃ and YSZ/Al₂O₃, *Mater. Sci. Eng. A*, 2008, **478**, p 264–269
26. C. Batista, A. Portinha, R.M. Ribeiro, V. Teixeira, M.F. Costa, and C.R. Oliveira, Surface Laser-Glazing of Plasma-Sprayed Thermal Barrier Coatings, *Appl. Surf. Sci.*, 2005, **9**, p 247–313
27. C. Ren, Y.D. He, and D.R. Wang, Preparation and Characteristics of Three Layer YSZ-(YSZ/Al₂O₃)-YSZ TBCs, *Appl. Surf. Sci.*, 2011, **257**, p 6837–6842

28. X.Q. Cao, R. Vassen, and D. Stoever, Ceramic Materials for Thermal Barrier Coatings, *J. Eur. Ceram. Soc.*, 2004, **24**, p 1–10

29. G.M. Pharr, Measurement of Mechanical Properties by Ultra-Low Load Indentation, *Mater. Sci. Eng.*, 1998, **A253**, p 151–159

30. G. Di Girolamo, F. Marra, C. Blasi, E. Serra, and T. Valente, Microstructure, Mechanical Properties and Thermal Shock Resistance of Plasma Sprayed Nanostructured Zirconia Coatings, *Ceram. Int.*, 2011, **37**, p 2711–2717

31. L. Wang, Y. Wang, X.G. Sun, J.Q. He, Z.Y. Pan, and C.H. Wang, Thermal Shock Behavior of 8YSZ and Double-Ceramic-Layer La$_2$Zr$_2$O$_7$/8YSZ Thermal Barrier Coatings Fabricated by Atmospheric Plasma Spraying, *Ceram. Int.*, 2012, **38**, p 3595–3606

32. X. Chen, Y. Zhang, X. Zhong, Z. Xu, J. Zhang, Y. Cheng, Y. Zhao, Y. Liu, X. Fan, Y. Wang, H. Ma, and X. Cao, Thermal Cycling Behaviors of the Plasma Sprayed Thermal Barrier Coatings of Hexaluminates with Magnetoplumbite Structure, *J. Eur. Ceram. Soc.*, 2010, **30**, p 1649–1657